SPE 99719

Upscaling of Foam Mobility Control to Three Dimensions

Busheng Li, George J. Hirasaki, and Clarence A. Miller, Rice University, Houston, TX

This paper was prepared for presentation at the 2006 SPE/DOE Symposium on Improved Oil Recovery held in Tulsa, Oklahoma, U.S.A., 22–26 April 2006.

Abstract

The applications of foam are 3-D on a field scale. However, most previous research focuses only on properties of foam in 1-D. Experiments were performed in 3-D, and the compositional reservoir simulator UTCHEM was modified to predict foam flow in 3-D.

The 3-D experiments demonstrated that, under similar experimental conditions, the mobility of foam in a 3-D tank is greater than that in a 1-D column. They also showed that foam greatly increases lateral gas distribution along the bottom of the tank and the average gas saturation for both homogeneous and heterogeneous packings with the effects being significantly larger in the latter case. The reservoir simulator UTCHEM was modified for foam flow. The foam simulation parameters were measured in 1-D sand columns and the simulator was modified to match the 1-D and 3-D experiments. The proposed model successfully history matched the homogeneous and heterogeneous 3-D sand tank experimental results for average gas saturation, gas injection rate, gas distribution and pressure profile along the tank diagonal 6 inches from the bottom.

The results of this study represent an advance in understanding of foam flow in 3-D. The simulator could be used to design a foam process in 3-D.

Introduction

Foam mobility difference in 1-D and 3-D. Foam is used for mobility control in aquifer remediation processes[1-4] and oil recovery operations[5-8]. Gas has low density and viscosity compared to other fluids like oil and water. So when gas is injected into the porous media, the gravity force will dominate its flow and the injected gas will tend to flow directly to the top of the porous media, results in a poor gas sweep in the horizontal direction along the bottom (Fig.1). Foam can reduce the mobility of gas by reducing the relative permeability and increasing the apparent viscosity thus increasing the gas sweep efficiency. However, though there were some field applications of foam, most of the previous laboratory researches on foam were in 1-D. The properties of 3-D foam have not been investigated yet. Tanzil[9] observed that the apparent viscosity of foam is greater in 3-D than in 1-D. His observation was based on a rough comparison between a 3-D field scale foam application and some 1-D column experiments in lab. No strict experiments were performed by him to demonstrate the difference between 1-D and 3-D. Nevertheless, the observed mobility difference of foam between 1-D and 3-D revealed how much error would result if one uses 1-D column foam experimental results to predict 3-D field application results. A foam simulation model developed from 1-D experimental results would not be applicable to simulate 3-D foam results. 3-D foam experiments are important for us to understand the flow properties of foam and a simulation model is also indispensable to simulate and predict 3-D foam flow behavior considering the complexity and difficulty of performing 3-D foam experiments in lab.

Foam generation and coalescence. Hirasaki *et al* [10]defined that foam in porous media is a dispersion of gas in liquid such that the liquid phase is continuous and at least some part of the gas phase is made discontinuous by lamellae. Previous studies showed that the main generation mechanisms of foam in porous media are capillary snap-off, lamella division and leave behind. Among them, lamellae generated from the former two mechanisms are mainly perpendicular to the gas flow direction and can block the gas flow, greatly reduce the gas mobility. So these two mechanisms are considered to be able to generate strong foam. Pressure gradient[11-14] is important in strong foam generation process. Higher ∇p can mobilize more stationary lamellae, set off the lamellae division process and generate more new lamellae which will block more of the gas flow paths. In porous media, the main coalescence mechanism of foam is capillary suction. Foam lamellae would break when capillary pressure reaches a limiting value[15], which is named the "limiting capillary pressure" P_c^*. The value of the limiting capillary pressure depends on many parameters including surfactant concentration, permeability and gas and liquid velocities.

Mobility of water and gas when foam is present. The relative permeability function of water is not directly influenced by the presence of foam[16-17]. Foam can only change the water mobility indirectly by changing the water saturation in porous media. For the flow of gas, foam can greatly reduce

the mobility of gas from two aspects. When foam is present, the gas relative permeability will be smaller than in conventional two-phase flow and gas apparent viscosity is larger because of the resistance to movement of lamellae. The reduction of gas relative permeability arises because only a fraction of the gas phase is actually flowing when foam is present, i.e., some gas is trapped. The increase of apparent gas viscosity comes from the flow of foam bubbles. Resistance to flow of the bubbles is greater than resistance to flow of gas when no lamellae are present because of the dragging of lamellae along the pore walls[18]. Combining these two effects, gas mobility is reduced significantly when foam is present, the stronger the foam, the lower the gas mobility.

Foam modeling. Foam texture (lamella density) determines the strength and mobility of foam and itself depends on many factors such as pore structure, heterogeneity, surfactant formulation, capillary pressure, flow rates, presence of non-wetting phase, etc. It is very difficult and complex to investigate the relation between foam mobility and these factors. There are many ways to model foam flow in porous media. Most of the models modify gas mobility when foam is generated. These foam models can be classified into four major groups. They are empirical and semi-empirical models, fractional-flow theory models, percolation (statistical networks) models and population balance models.

Among all these foam models, the population balance method is the most comprehensive approach to fully describe foam mechanisms. Several investigators[19-20] have used this approach in modeling foam in porous media. The significant achievement of the method is accounting for non-Newtonian gas mobility with respect to bubble population dynamics. In this approach, foam texture is explicitly taken into account. They solve a number of equations to describe lamella generation and destruction processes. The effective foam viscosity is determined by the calculated lamella density. The shortcoming of this model is its complexity: many parameters need to be determined in this approach by performing corresponding experiments. Attempts were performed to simplify the population-balance model by some other investigators. Hatziavramidis *et al*[21] proposed a simplified population-balance model. In their model, when the foam is weak, only the relative permeability of the gas was modified. In the case of strong foam, the viscosity of the gas was also modified. Their model was applied on steam foam and incorporated into a thermal simulator, THERMS. Bertin *et al*[22] offered a simplified model of the full population balance model of Kovscek *et al*[20]. Foam texture was calculated using a bubble-population correlation and represented as a function of porosity, permeability, gas saturation, the limiting capillary pressure and the flowing foam fraction. The effective gas viscosity was modified when foam was present. This model was shown to give satisfactory results in modeling transient core experiments. Friedmann *et al*[23] proposed a foam model in which the calculation of foam viscosity including a geometric factor and a reference velocity. In later sections of this paper, a foam model will be discussed based on the discussion of the models proposed by Bertin *et al*[22] and Friedmann *et al*[23].

Objective of this research. The purpose of this paper is to investigate the flow behavior of foam in 3-dimensions, compare the difference between air/water and foam cases and develop a foam model to simulate both 1-D and 3-D foam flow.

Experimental

Configuration of the 3-D tank. A 3-D sandpack was designed and constructed for the 3-dimensional foam experiments. Fig.2 shows a photograph of the empty tank with wells and sampling tubes. The tank has glass walls for its four sides. Steel frame is used in the corners and edges to make the tank strong enough to hold the experimental pressure. The actual scale of the tank is 2ft×2ft×2.5ft with a height 2.5ft. But we still call it '2x2x2 ft tank' because the extra 0.5 ft in its height was not packed by sand in our 3-D experiments. The term '2x2x2 ft' here only means the porous media size inside the tank.

There are nine sampling tubes and four injection/production wells in the tank. Fig. 3 gives sketches of the side and top views of the sand tank. The sampling tubes are placed in lines and in each line, they are 0.5 ft from each other. The distance from line to line is also 0.5 ft. In each of these sampling tubes, there are four sample openings. The heights of these openings are 0, 0.5, 1 and 1.5 ft from the bottom of the tank. Four individual plastic tubes connect these openings to the outside of the tank. During experiments, these sampling tubes can be used to get information such as gas and surfactant solution distribution inside the tank.

The tank has one injection well and three production wells as shown in Fig. 3. The diameter of these wells is 1.75 inch. To keep sand out of these wells, these wells are wound with 200 mesh stainless steel screen. The injection well is 3.5 inches high, and the three production wells are 2 ft high. All the production wells have their outlets at the bottom of the tank but use a ¼" inch stainless steel tube to make the flow outlet to be at the same level as the height of the sand pack. This is just to keep the pressure potential inside the production wells at hydrostatic pressure and simulate an unconfined aquifer.

A 150 mesh screen and a ~200 lbs overburden are put on the top of the sand pack, which is to keep the sand from flowing upwards during gas injection at high pressure. The ~200 lbs overburden can increase the maximum possible injection pressure of the sand pack without fluidizing the sand.

Two sand pack formations. Silica sands were used and two different sand packings were tested. Fig. 4 shows a drawing of these two packings. One is a homogeneous pack using sand of a permeability about 40 darcy. The other is a heterogeneous pack, where two layers of high permeability sand (200 darcy) were packed in the lower part of the tank. Both of these layers are 2.5 inch thick. One is located 2.5 inches and the other 7.5 inches above the bottom of the tank. The rest of the tank is packed with 40 darcy sand.

Experimental procedures. Fig. 5 shows the experimental procedure for the 3-D tank experiments. A pressure transducer was connected to the injection line to measure the injection pressure. A water manometer was installed at the injection line to monitor the air injection pressure. This manometer can hold

2 psig pressure. When injection pressure exceeds 2 psig, water will be blown out to avoid fluidizing the sand in the tank. Two air flow controllers were installed in the injection line. Their flow rate ranges are 0.1~10LPM and 1~100LPM. A three-way valve was installed in the injection line. It can switch between these two controllers during the experiments to get the desired flow rate. Three pressure transducers were installed along the diagonal cross section of the tank at points 0.5 foot from the bottom of the tank. P1, P2 and P3 of Fig. 5 indicate the locations of these transducers.

Both air/water and foam experiments were performed in the sand tank. The tank was filled with surfactant-free water or surfactant solution before each experiment. The surfactants solution was a 1:1 mixture of 0.05%(wt)CS-330 and 0.05%(wt)C13-4PO. Air was injected into the tank either continuously or intermittently. In most of the experiments, the injection pressure was kept constant by adjusting the air injection flow rate. The results of air/water and foam experiments are compared.

Experimental Results

Injectivity difference between air/water and foam. Fig 6 and 7 show the plots of gas injection time vs. gas injection rate for the air/water experiments in the homogeneous and heterogeneous tank. The experiments were performed at a constant injection pressure ~0.8 psig over hydrostatic pressure. From the plotted curve we can see that in both of the homogeneous and heterogeneous experiments, the gas injection rate reached a steady state after a short time of gas injection. At steady state, the injection rate was around 30 LPM (Liter Per Minute) for both of these two experiments. Fig 8 and 9 show the curve of the gas injection rate vs. gas injection time for the foam experiment performed using the same injection pressure as in the air/water experiment. Fig. 8 is the results from the homogeneous pack and Fig. 9 is the results from the heterogeneous pack. From the plots we can see in the foam cases, at steady state, the gas injection rate was about 1 LPM for both the homogeneous and heterogeneous sand packs. Comparing to the air/water case, the steady state gas injection rate when foam is present was about 1/30 of the without foam cases. Also, we can find that the steady state injection rate can be reached with fewer PV of gas injected in foam experiments. For example, in the homogeneous sand pack experiments, in foam case, the gas needed to reach the steady state was about 6 times less than in air/water case (only 0.5 PV needed in foam case but 3PV needed in air/water case).

Gas sweep efficiency. From the sample tubes we obtained the gas fraction flow information in the sand tank. Fig.10 gives the diagonal cross section gas fraction flow contour plots for air/water and foam experiments in the homogeneous tank. The difference between air/water and foam is phenomenal in these diagonal plots. From the plots we can see that in the air/water case after 6 PV gas injected, there was still quite a lot of the bottom of the tank left uncontacted by gas. Most of the injected gas tended to flow upwards and then out of the top of the tank. In the foam case, after only about 0.37 PV gas was injected, the area contacted by gas at the bottom of the tank was already almost as large as in the air/water case after 6 PV gas was injected. Gas continued to propagate horizontally along the bottom of the tank with the injection of more gas. After 2 PV gas was injected, almost all the bottom of the tank was contacted by gas.

Fig.11 shows a comparison of the gas fractional flow contour plots along the diagonal cross section in the heterogeneous tank. From these plots we can see, just similar as in the homogeneous tank, in the air/water case, the gas flow direction was mainly upwards and the shape of the flow area resembled a cone. In the air/water case, after even 6 PV gas was injected, most of the lower part of the tank was still not contacted by gas. On the contrary, in the foam case, gas flow was very different with a much stronger lateral component. Most of the lower part of the tank was contacted by gas after about 1 PV of gas was injected. After 2 PV gas was injected, almost all the tank was swept by gas.

These comparisons showed that, in both the homogeneous and heterogeneous system, foam greatly increased the gas sweep efficiency. Without foam, it is very difficult to sweep the whole tank, especially in the near bottom part or lower permeability regions.

Gas saturation. Another big difference between air/water and foam results is the average gas saturation in the tank. In the homogeneous sand pack experiments, in the air/water case, the average gas saturation was only about 23% after 6 PV gas was injected. But in the foam case, the average gas saturation was as high as 66% with only about 1 PV gas was injected. The average gas saturation in the foam case was about three times higher than in the air/water case with only 1/6 amount of gas was injected. The average gas saturation in the foam case was even higher after more PV gas injected. After 2 PV gas was injected in the foam case, the average gas saturation reached about 80%, which was about four times higher than in the air/water case.

In the heterogeneous sand pack experiments, the difference was more apparent. In the air/water case, after 1 PV gas was injected, gas saturation was only 18% and after even 6 PV gas was injected, gas saturation was still low (about 39%). On the contrary, in the foam case, after 1 PV gas was injected, gas saturation was as high as 82% and after 2 PV gas was injected, gas saturation increased to about 92%. The saturation difference between air/water and foam cases show that most of the injected gas flowed out of the tank when there was no foam but a much larger percent of the injected gas can be trapped in the tank when foam was present. Foam greatly increased the average gas saturation in the sand pack.

Diagonal pressure profile. Fig.12 A and B show the pressure profile along the diagonal cross section of the tank 6 inch from the bottom in the heterogeneous sand pack. In air/water case, most of the pressure drop was around the injection well. P1 was the highest pressure drop among the three measured pressure drops. P2 and P3 were negligible compared to P1. In foam case, P1 was not the highest pressure drop. Instead, P2 was higher than P1 and P3. The pressure profiles demonstrated that in air/water case, there was little flow except near the injection well. In foam case, gas flowed throughout the cross section of the tank. The fact that P1 was lower than P2 also told us that foam had lower strength around the near well region than in the further region. We observed this

phenomenon not only in this heterogeneous foam experiment, but also in all the other 3-D foam experiments. Shear thinning effect of foam under high injection rate may be the reason for this phenomenon. This shear thinning effect is included in our foam model and will be discussed more in the latter part of this paper. The proposed simulation model successfully history matched the pressure profile by taking into account of the shear thinning effect of foam.

Comparison of different injection strategies. Two other kinds of foam experiments were performed in both of the homogeneous and heterogeneous 3-D tank to test the effect of different injection strategies. One was performed using an intermittent gas injection method: gas was injected into the tank in a 5 minutes on and 5 minutes off cycle. The other one was performed using a lower injection pressure at about 0.4 psig over hydrostatic pressure, which was about a half of the constant injection pressure (0.8 psig) chosen in our former foam experiments.

Let us first compare the experiments performed in the homogeneous sand pack. Fig. 13, 14 and 15 show the gas fractional flow contour plots for the four sampling layers after 1 PV gas were injected in the continuous gas injection, intermittent gas injection and low injection pressure cases correspondingly. For Fig. 15, it was actually a constant injection rate experiment (0.39LPM), but the injection pressure reached steady state very quickly in this experiment and stayed at about 0.4 psig. So, it can also be considered as a low injection pressure (0.4 psig) foam experiment. From these plots we can see, in the constant injection pressure, continuous air injection case, gas contacted about 4/5 of the bottom layer after 1PV gas was injected. The average gas saturation was about 66% after 1 PV gas was injected. In the constant injection pressure, intermittent air injection case, almost all the bottom of the tank was contacted by gas. Gas also contacted more than 90% area of the upper part of the tank. The average gas saturation was about 73%, which was significantly higher than in the continuous air injection foam case. In the low injection pressure case, gas contacted only about 1/5 of the bottom layer after 1PV gas was injected. For the upper layers, gas sweep was also not good. Gas cannot propagate far horizontally and most of the injected gas flowed out from the top of the tank. One can also tell this from the gas saturation in the tank, which was only 37% after 1 PV gas was injected, much less than that in the other foam experiments.

Fig. 16, 17 and 18 show the results from the heterogeneous sand pack after 1 PV gas was injected in the continuous gas injection, intermittent gas injection and low injection pressure cases correspondingly. By comparing Fig 16 and 17, we find that, in the heterogeneous sand pack, the gas sweep results of the intermittent injection case were very similar to those of the continuous injection case. Both had good gas sweep efficiency in the lower part of the tank. But strictly speaking, the intermittent injection case had a better sweep efficiency than the continuous case, though the difference between them is slight. For example, after 1 PV gas was injected, in the intermittent case, the layer 0.5 ft from the bottom was completely contacted by gas. But in the continuous injection case, there were still some areas where the gas fractional flow was less than 100%. For the results of lower injection pressure in Fig.18, we can see that though the gas contacted area was relatively large in this experiment, the gas sweep efficiency was obviously worse than in the 0.8 psi foam experiment (Fig. 16). In the 0.4 psi case, after 1 PV gas was injected, there was still quite a lot area in the lower two layers which had not been contacted by gas. In the 0.8 psi case, almost all of the lower part of the tank was contacted by gas. This can be easily identified from the color of the contour plots. In the 0.4 psi case, there is a large dark area in the bottom, which means low gas fractional flow there. But in the 0.8 psi case, almost all the bottom of the tank is white, which means a very high value of gas fractional flow.

By comparing all the experimental results for different injection strategy and in different sand packs, the intermittent gas injection method is demonstrated to be the best injection strategy, which can result in the best gas distribution and the highest gas saturation.

Simulation Approach

Model description. The transport of foam in porous media is governed by Darcy's Law:

$$u_g = \frac{k k_{rg}^f}{\mu_g^f} \nabla p \tag{1}$$

Flowing foams occur when snap-off or lamella division produces discrete bubbles. When foam is present, as discussed earlier, both the gas relative permeability k_{rg}^f and the gas apparent viscosity μ_g^f are affected.

a. Equation of k_{rg}^f. The relative permeabilities k_{rl} for liquid and gas phases can be calculated using the Corey model as follows:

$$k_{rl} = k_{rl}^0 \left(\frac{S_l - S_{rl}}{1 - S_{rl}} \right)^{e_l} \tag{2}$$

Where k_{rl}^0, S_l, S_{rl}, e_l are the relative permeability endpoint, saturation, residual saturation and exponent of phase *l*. As we mentioned earlier, the liquid relative permeability is the same function of liquid saturation either with or without foam. However, gas relative permeability, k_{rg}^f, is changed.

Falls *et al*[24] suggested that the effective foam permeability k_{rg}^f is reduced proportionally to the flowing gas fraction x_f :

$$k_{rg}^f(S_g) = x_f k_{rg}(S_g) \tag{3}$$

However, the fraction of gas that is flowing is a complex function of velocity, saturation, and capillary pressure. It is not easy to determine this function by simple experiments. Since the reason for the changing of gas relative permeability is the increased gas trapping inside the porous medium, we propose

a simpler way to account for this: we simply increase the gas residual saturation when calculating the gas relative permeability:

$$k_{rg}^{f} = k_{rg}^{0}\left(\frac{S_g - S_{rg}^{f}}{1 - S_{rg}^{f}}\right)^{e_l} \tag{4}$$

When foam is weak, which means the flowing gas fraction is high, the value of S_{rg}^{f} should be lower compared to the value of S_{rg}^{f} in strong foam. The value of S_{rg}^{f} can be determined by doing 1-D sand pack experiments.

b. Expression of μ_g^f. Friedmann *et al*[23] used the following expression for gas apparent viscosity when foam is present:

$$\mu_g^f = \mu_g F_g k^{3/2} n_f (v_g / v_{ref})^{n-1} \quad \text{for} \quad \mu_g^f > \mu_g$$
$$\text{and} \quad \mu_g^f = \mu_g \quad \text{for} \quad \mu_g^f \le \mu_g \tag{5}$$

where μ_g is gas viscosity without foam, F_g is a geometric factor and the last term accounts for the shear-thinning nature of the foam. In their simulation approach, n_f is the foam texture and is calculated by population-balance equations, v_g is the interstitial gas velocity and v_{ref} is a reference velocity beyond which the shear thinning effect occurs. *n* is the exponent for the shear thinning effect. However, to solve a population-balance equation, many parameters need to be determined. These parameters are not easy to determine, and so it is not very convenient to apply the equation to field situations. Here, based on their thoughts, instead of solving the population-balance equation, we seek to find some population correlation equation to calculate μ_g^f.

Bertin *et al*[21] suggested a bubble-population correlation model to calculate foam texture n_f:

$$n_f = \left(\frac{180(1-\phi)^2}{\phi^3}k\right)^{-3/2} S_g x_f \left(\frac{P_c^* - P_c(S_w)}{P_c(S_w)}\right) \tag{6}$$

He considered the limiting capillary pressure effect in his model. The lamellae become more fragile when capillary pressure increases and are destroyed when P_c reaches its limiting value P_c^*. Capillary pressure is a function of gas saturation. So in general, we can simplify Eq.(6) into the following way:

$$n_f = C_{nf} F(S_g) \tag{7}$$

where C_{nf} is a constant coefficient and $F(S_g)$ is a function of S_g. It implies that n_f is a function of S_g.

Now we need to find a detailed expression for $F(S_g)$ and then for n_f. Let's consider a foam generation process when gas invades the porous medium. Fig. 19 shows a sketch of how the value of n_f would change with the changing of S_g.

When $S_g = 0$, which means there is no gas inside the porous medium, of course there will be no foam texture, then we can get $F(S_g)$ =0, n_f =0 and in this initial no foam region,

$$\mu_g^f = \mu_g \tag{8}$$

With the increasing of gas saturation, lamellae are generated in the porous medium. During this period, the foam generation rate is greater than the foam coalescence rate. We can call it the lamella density accumulating region. The lamella density value, n_f, increases in this region:

$$n_f = C_{nf}\left(\frac{S_g}{S_{gm}}\right)^m \tag{9}$$

Substituting Eq.(9) into Eq.(5) and combining the coefficients $k^{3/2}C_{nf}$ into a new coefficient $C_{\mu f}$, and use gas superficial velocity instead of interstitial velocity, we can get the expression for μ_g^f in this region:

$$\mu_g^f = \mu_g F_g C_{\mu f}\left(\frac{S_g}{S_{gm}}\right)^m (u_g / u_{ref})^{n-1} \tag{10}$$

With the lamella density continuously accumulating, more and more lamellae are generated inside the porous medium, and the lamella coalescence rate will increase. When the gas saturation is greater than some particular value, S_{gm}, the foam generation rate and coalescence rate will be equal to each other. For simplicity we just assume that they remain equal until gas saturation reaches the critical gas saturation S_g^* at which $P_c(S_g^*) = P_c^*$ and the rate of coalescence is greater than the rate of generation. During this period, n_f reaches its maximum value and remains a constant. We can call it lamella density steady state region. In this region, the gas saturation range is $S_{gm} < S_g \le (S_g^* - \varepsilon)$ and

$$n_f = C_{nf} \tag{11}$$

The expression for μ_g^f is then:

$$\mu_g^f = \mu_g F_g C_{\mu f} (u_g / u_{ref})^{n-1} \tag{12}$$

When $S_g > (S_g^* + \varepsilon)$, the capillary pressure in the porous medium is greater than the limiting capillary pressure.

According to the limiting capillary pressure theory, foam would not exist and we will get $n_f = 0$ and $\mu_g^f = \mu_g$ again.

Between the lamella density steady state region and the no foam region, we defined a foam breaking transient region. Gas saturation is between $(S_g^* - \varepsilon) < S_g \le (S_g^* + \varepsilon)$ in this region and:

$$n_f = C_{nf}\left(\frac{S_g^* + \varepsilon - S_g}{2\varepsilon}\right) \tag{13}$$

and $$\mu_g^f = \mu_g F_g C_{\mu f}\left(\frac{S_g^* + \varepsilon - S_g}{2\varepsilon}\right)(u_g / u_{ref})^{n-1} \tag{14}$$

Here we defined and discussed four foam regions: 1. lamella density accumulating, 2. lamella density steady state, 3. foam breaking transient, 4. no foam region. Actually in our 1-D column and 3-D sand tank experiments, we only observed the first two regions. In other words, the generated foam is stable enough and didn't break under our experimental conditions. Our investigation and simulation are basically thus limited to these first two regions. But we still list the proposed equations for the last two foam regions here for completeness of the foam model.

Model summary. In this foam model, there are 9 parameters from these equations: S_{rg}^f, S_{gm}, $C_{\mu f}$, u_{ref}, m, n, F_g, S_g^* and ε

Among these parameters, S_g^* and ε are parameters for the foam breaking transient region and the no foam region. Because in our experiments we did not observe these two foam states, we did not try to determine these two parameters in our experiments and just focused our efforts on determining the parameters in the first two foam states.

Among the remaining parameters, S_{rg}^f, S_{gm}, u_{ref}, m and n can be determined by performing column foam experiments. $C_{\mu f}$ is a coefficient which combines the effects of pressure gradient, permeability and surfactant concentration. Its value represents the strength of the generated foam at steady state and can also be determined by 1-D column experiments. F_g is a geometry factor which represents the effects of flow dimensions on foam strength. For simplicity, we just define F_g to equal to one in 1-D foam flow. From our experimental observation among 1-D and 3-D experiments, the value of F_g is different for 1-D and 3-D foam flow. The F_g value for 3-D foam flow is estimated by doing history match simulations.

The foam model is incorporated into the reservoir simulator UTCHEM and all the simulations in this paper were performed using this modified simulator.

Determination of simulation parameters. Some 1-D column foam experiments were performed to determine the simulation parameters for the simulation model. Fig. 20 shows the set up of the 1-D column experiments. The horizontal column is 1 ft long and packed with 40 darcy or 200 darcy sand. Gas or surfactant solution can be injected from one end of the column and fluids produced from the other end. A pressure transducer is used to record the injection pressure when needed.

a. Residual saturation with foam. To determine the residual gas saturation inside the column when foam is present, the column was pre-filled with surfactant solution and then gas was injected into the column at a constant injection pressure. After all of the column was swept by foam and the injection rate reached its steady state, gas injection was turned off and surfactant solution was re-injected into the column under the same constant injection pressure. When the injected liquid volume equals to the produced liquid volume in some time interval, by doing a material balance of the total injected and produced liquid volume, we can calculate the residual gas saturation inside the column. The gas residual saturations for both the 40 darcy and 200 darcy sands were measured. For each of these sands, two different injection pressures, (0.2 psi and 0.4 psi) experiments were performed. Fig. 21 shows the measured gas saturation vs. injected liquid PV. From the results we can see that for 40 darcy sand and 200 darcy sand, the gas residual saturation when foam was present was about 40% and 70% correspondingly, which did not change much with the change of injection pressure.

b. Parameters (u_{ref} and n) of shear thinning effect. From Eq.(10), we can get the following relationship:

$$\ln(\mu_g^f) - (n-1)\ln(u_g / u_{ref}) = \ln(\mu_g F_g C_{\mu f}) - m\ln S_{gm} + m\ln S_g \tag{15}$$

From Eq.(15), we can find that when the value of S_g is a constant, the right side of the equation will be a constant and there will exist a linear relationship between $\ln(\mu_g^f)$ and $\ln(u_g)$. From the slope of the plot we can get the value of n. To determine u_{ref} and n, the column was filled by surfactant solution first and then gas was injected into the column in a high injection pressure, i.e. 7 psig. After all the column was swept by strong foam and the average gas saturation in the column did not change any more, gas injection was turned off for several minutes to let the inside pressure of the column drop to zero. Then gas was re-injected into the column at different injection rates. The pressure drop for each injection rate was recorded and the corresponding effective gas viscosity was calculated using Eq.(1) and (4). Both the 40 darcy and 200 darcy sands were tested to measure the shear thinning effect parameters.

Fig. 22 and Fig. 23 show the plot of gas velocity vs. μ_g^f for 40 darcy and 200 darcy sand column correspondingly. From Fig. 22 we can see when gas velocity is less than about 2 ft/day, there is no shear thinning effect. When the velocity becomes greater than 2 ft/day, the shear thinning effect reduces the value of μ_g^f and the value of the power law exponent, n, is about 0.2. So for 40 darcy sand, we can get

$u_{ref} = 2$ ft/day and $n = 0.2$. Accordingly, from Fig. 23 we can get $u_{ref} = 6$ ft/day and $n = 0.4$ in the 200 darcy sand column.

c. Parameters (S_{gm}, m and $C_{\mu f}$) of gas saturation effect. The determination of m depends on which kinds of experiments are performed. If the experiment is performed under constant injection rate, which means u_g is a constant, then there will be a linear relationship between $\ln(\mu_g^f)$ and $\ln S_g$. The slope of the plots will be m. For constant injection pressure experiments, the average gas saturation in the column and the injection rate can be recorded as a function of time and the corresponding values of μ_g^f can be calculated from these records. A linear relationship will exist between $\ln(\mu_g^f) - (n-1)\ln(u_g / u_{ref})$ and $\ln S_g$. The slope of this plot will also be m.

Fig. 24 shows the relationship between μ_g^f and S_g in a 0.4 psi constant injection pressure foam experiment for the 40 darcy sand column. From this figure we can see that with increasing gas saturation, foam effective viscosity also increased. The value of μ_g^f kept increasing when S_g was less than 0.8 and increased dramatically when S_g was between 0.75 and 0.8. But when S_g was greater than 0.8, the value of μ_g^f was approximately leveled off. So for this experiment, the value of S_{gm} should be around 0.8. When $S_g < S_{gm}$, foam generation rate is greater than foam coalescence rate and the value of μ_g^f increases. When $S_g > S_{gm}$, these two rates are almost equal and μ_g^f is approximately constant.

Also, from Fig. 24, we can find that at steady state, the gas saturation is more than 80% which is greater than S_{gm} and the gas superficial velocity is less the reference velocity 2 ft/day. No shear thinning effect if velocity is under that value. So, from Eq. (12), at this time, we can get:

$$\mu_g^f = \mu_g F_g C_{\mu f} \tag{16}$$

Since F_g is a geometry factor which represent the mobility difference between 1-D and 3-D, it would not hurt for us to define its value to be one in 1-D foam flow. In latter part of this paper, we will talk about its value in 3-D which is determined from 3-D history match simulations. Then from Eq.(16) and since the value of the steady state effective viscosity was about 90 cp (Fig.24), we can calculate the value of $C_{\mu f}$. If we use 0.02 cp as the value of μ_g , $C_{\mu f}$ is around 4500. Moreover, Fig. 25 shows the plot of the relationship of $\{\ln(\mu_g^f) - (n-1)\ln(u_g / u_{ref})\}$ vs. $\{\ln S_g\}$ (for this case, n=0.2, as shown in Fig.22). According to Eq. (15), for constant injection pressure experiments, there should be a linear relationship between them and the slope of it will be the value of m. From the plots we can see the linear relationship exists and the value of m is around 5.0.

A 0.2 psi constant injection pressure experiment was also performed in this 40 darcy column. Similar plots as in Fig.24 and 25 can be obtained from the experimental results and the values of S_{gm}, m and $C_{\mu f}$ can be determined correspondingly. Experiments were also performed in the 200 darcy sand column to determine the value of these parameters in it. Table 1 lists the parameters we determined from the 1-D column experiments for 40 darcy and 200 darcy sands under 0.4 psi and 0.2 psi constant injection pressure.

Simulation results

a. 1-D column. The experimentally determined foam model parameters were used to simulate the corresponding 1-D column foam experiments. Fig. 26 to 29 show the simulated injection rate compared to the experimental result for 40 darcy and 200 darcy sands under 0.4 and 0.2 constant injection pressures. The simulated results matched the experimental results. Table 2 compares simulated and experimental average gas saturations. The simulated gas saturation matched the experimental results. From these comparisons we can see the 1-D column experimental results can be simulated and matched by using the proposed foam model and the determined parameters.

b. 3-D homogeneous sand pack. In the history match simulation of the 3-D homogeneous foam experiments, the overall pressure gradients in the experiments were used as the comparison standard to compare to the corresponding 1-D column experiments. For example, in the 0.8 psi constant injection pressure tank experiment, the overall pressure gradient was about 0.4 psi/ft, which was the same as the pressure gradient in the 0.4 psi constant pressure 1-D column (1 ft) experiment and the parameters obtained from this 1-D column experiment will be used to simulate the 3-D tank experiment.

In the 3-D sand tank simulations, we kept all the parameters the same as in the corresponding 1-D column simulations except for the value of F_g .This value represents the effect of flow dimension on foam strength. To get the best match simulation results, we needed to choose a smaller F_g value for the tank simulations than for the 1-D column simulations. In 1-D foam flow, for convenience, we defined this value to be 1.0. In 3-D simulations, we found this value must be set to be around 0.21 to get the best match results, as is seen below. The simulation parameters for 3-D foam experiments are listed in Table 3.

For the 0.8 psi constant injection pressure 3-D foam experiment, Fig. 30 shows the simulated injection rate compared to the experimental data. Agreement is good for both the rate and the average gas saturation. After around 1 PV gas was injected, the simulated average gas saturation inside the tank was about 69% and the experimental data is 66%. Fig. 31 shows the simulated gas fractional flow contour plots compared to the experimental data. After about 1 PV gas was injected, gas contacted more than 75% of the cross sectional

area of the tank. Fig.32 shows the simulated diagonal cross section pressure profile compared to the experimental data. From the pressure profile we can see that the highest pressure drop is around the middle part of the tank. The region near the injection well (p1) has a lower pressure drop compared to the middle region (p2).

For the lower injection pressure (0.4psi) 3-D foam experiment, Fig. 33 shows the simulated gas fractional flow contour plots match the experimental data well. The average gas saturation values are also in good agreement. In this experiment, the average gas saturation after about 1 PV gas injected was about 37%, compared to the simulated result of about 33%. Fig. 34 shows the comparison between the simulated pressure profile and the experimental data. Just as in the 0.8 psi foam experiment, the pressure drop near the injection well (p1) is lower than that in the farther region of the tank (p2).

c. 3-D heterogeneous sand pack. History match simulations were also performed for the 3-D heterogeneous foam experiments. As in the homogeneous sand pack simulations, the overall pressure gradients in the experiments were also used as the comparison standard between 1-D and 3-D. The simulation parameters for the heterogeneous results are also shown in Table 3.

Fig.35 shows the comparison of simulated and experimental injection rates for the 0.8 psi constant injection pressure experiment in the heterogeneous sand pack. The simulated average gas saturation after 1 PV gas injected was about 73%, while the corresponding experimental result was about 82%. Fig. 36 shows the comparison of the gas fractional flow contour plots after 1 PV gas was injected. Fig. 37 shows the simulated pressure profile compared to the experimental data. The strongest foam region is in the middle part of the tank.

Another history match simulation was performed to simulate the 0.4 psi constant injection pressure foam experiment. Fig. 38 shows the comparison of simulated and experimental injection rates for the 0.4 psi constant injection pressure experiment. Fig. 39 shows the comparison of gas fractional flow plots after 1 PV gas injected. The simulated average gas saturation after 1 PV gas injected was about 68%, and the experimental result was about 60%. Fig. 40 shows the simulated and experimental pressure profiles. The simulated pressure profile matched the experimental results. The simulated highest pressure drop was also in the P2 region, just as the result from the experiment.

Summary and Discussion

a. 3-D Experiments. In air/water experiments, because of the low density and viscosity of gas, the injected gas flowed mainly upwards and much of the bottom region was left uncontacted. For a heterogeneous system, the uncontacted region was larger because in such system, the high permeability region acted as a shortcut for the gas flow and then less gas can flow into the low permeability region at the bottom of the tank. In foam experiments, foam reduced gas mobility in either the homogeneous or heterogeneous sand packs. From all these comparisons among air/water and foam, we found that foam can greatly increase the gas sweep efficiency and average gas saturation in both the homogeneous and the heterogeneous sand packs. Also, at steady state, foam will result in a lower inject rate compared to the air/water case, the ratio between foam and air/water is about 1/30 for similar injection pressures experiments, either in the homogeneous or the heterogeneous pack.

Moreover, the effect of foam is more apparent in the heterogeneous pack than in the homogeneous pack. The average gas saturation was higher in the heterogeneous pack than in the homogeneous pack. After 1 PV gas was injected, the average gas saturation in the heterogeneous tank was about 82%. Compared to the 66% gas saturation in the homogeneous tank after 1 PV gas was injected, the gas saturation in the heterogeneous sand pack increased by 16% because of the effect of heterogeneity. The gas contacted area in the heterogeneous pack was also larger than in the homogeneous pack. By comparing Fig 13 and 16, 14 and 17, 15 and 18, we can easily find the gas sweep in the lower part of the sand tank was apparently larger in the heterogeneous cases. This can be explained from the foam generation mechanisms in porous media. In a homogeneous system, lamella division is the basic foam generation mechanism which happens when a moving lamella train encounters a branch in the flow path. The mechanism of snap-off is not the main mechanism to generate strong foam in homogeneous system because there is no permeability contrast in it and repeated snap-off is unlikely in such a system. In a heterogeneous system, both lamella division and snap-off play important roles in determining the strength of generated foam. According to Tanzil *et al*[25], when gas flows from a low permeability region to a high permeability region and when there is a permeability contrast of more than four, lamella snap-off will occur because of the difference of the capillary pressure in these two regions. Lamellae generated along the boundary between the low and high permeability sands will block flow paths of gas and hence increase its apparent viscosity in the high permeability regions. More gas can then flow into the low permeability region. The effect of foam was then more apparent in a heterogeneous system than in a homogeneous system.

Shi *et al*[26] pointed out that injection well pressure is the key to avoid gravity segregation of gas. Our 3-D experimental results also demonstrated that the injection pressure is very important to obtain a good gas sweep and high gas saturation. In our experiments, the worst case in gas distribution and saturation was in the lower injection pressure cases (0.4 psi above hydrostatic pressure, about half of the pressure in the other foam experiments). In these cases, because of the lower injection pressure, the pressure gradient was lower and there was no strong foam generated. So the gas flow was dominated by gravity, and most of the gas flowed upwards and did not contact much of the bottom of the tank. To obtain best results, in both of the homogeneous and heterogeneous sand packs, the injection pressure should be high enough to generate strong foam, which promotes the horizontal flow.

Also, for a constant injection pressure experiment, the intermittent injection method provides better gas sweep efficiency and higher average gas saturation than the continuous injection method. The shut-in intervals during the experiment allow the sands to be partially re-saturated, and this can keep the foam from drying and then breaking. In the

heterogeneous pack, the effect of intermittent injection is not as great as in the homogeneous pack. Nevertheless, the intermittent injection method still benefits gas sweep efficiency and average gas saturation in the tank, either in the homogeneous pack or the heterogeneous pack.

b. Simulations. Foam generation is a complex process. For different experimental conditions, i.e. different surfactant concentrations, different injection pressures or injection rates, the generated foam strength may vary. The foam simulation model proposed in this paper simulates foam flow in 3-D by doing only 1-D experiments to evaluate key simulation parameters. In this model, when foam is present, both the gas relative permeability curve and the apparent viscosity of the gas are changed. The gas relative permeability curve changed because of the increased trapped gas saturation. The apparent viscosity is defined as a function of gas saturation, gas velocity and flow dimension. Most of the simulation parameters can be determined by 1-D column experiments and then applied to 3-D foam simulations under similar conditions.

Just as shown in Table 3, a F_g value of about 0.21 was found to be needed to history match the 3-D homogeneous tank results. This represents an effective decrease in foam strength in 3-D due, among other things, to the existence of more pathways for gas to flow through the sand.

Taking this F_g value between 1-D and 3-D, additional simulations were performed for the heterogeneous sand pack experiments. From the history match with the experiments, we found that foam strength is increased because of heterogeneity. Table 3 also lists the parameters which were chosen for the best match simulations for the heterogeneous experiments. In the high permeability layers, the foam strength parameter $C_{\mu f}$ increased about 3 times owing to snap-off which occurred as gas entered these layers from the underlying low-permeability layers. For example, in the 0.8 psig experiments, in the 200 darcy column experiment, $C_{\mu f}$ is found to be about 1200, but in the 3-D heterogeneous simulation, keeping F_g as 0.21, a higher $C_{\mu f}$ value (3100) is needed which is about 3 times larger than the 1-D column value. In the low permeability region, the value of $C_{\mu f}$ increased by about 50% for one of the two experiments but was the same as for the homogeneous tank in the other experiment. The results here showed that the heterogeneity can increase the foam strength not only in the high permeability region but also in the low permeability region.

c. Extend to field scale simulation. For field scale simulation, we use a pressure gradient which is calculated by using the injection pressure (over hydrostatic) divided by 2 ft as a comparison standard to the 1-D column. For example, for a 8 psi over hydrostatic pressure injection case, the calculated pressure gradient will be 4 psi/ft and then we will choose the simulation parameters from the corresponding 4 psi/ft 1-D experimental results. The reason we choose 2 ft here is because it is the same dimension as the tank in our lab and the F_g relationship we found is based on this dimension.

Some higher injection pressure foam experiments were performed in 1-D column. Fig. 41 shows a plot of the change of the $C_{\mu f}$ value with the change of the pressure gradient. From this plot we can see in both the 40 darcy and 200 darcy sand column, when the pressure gradient is higher than about 1.6 psi/ft, the value of $C_{\mu f}$ levels off. For the other simulation parameters, they also do not change much with the increasing of the pressure gradient[27]. So in general, we found that the simulation parameters will keep the same when the pressure gradient is higher than some value, i.e. 1.6 psi/ft in our cases.

The other issue we need to consider in a field simulation is the shear thinning effect (Fig. 22 and 23) between the well bore and the grid block. In the 3-D tank simulations, we modeled the shear thinning effect among grid blocks. Because the pressure difference between the well bore and the grid block which contains the injection well in the 3-D tank is very small, the shear thinning effect is also small between them and can be ignored. But in the field simulation, because the grid block is much bigger than the well bore, there will be a significant pressure/velocity difference between the well bore and the grid block in the simulation. We need to consider the shear thinning effect between them. Following the discussing of Bondor *et al*[28] on a well model of polymer injection, we added a negative, viscosity dependent apparent skin factor Sp in the well model to represent the non-Newtonian effects between the well bore and the gridblock in our foam case. The injection rate will then be a function of this apparent skin factor due to non-Newtonian effects. We can get higher injection rate because of this non-Newtonian effect.

Fig. 42 shows a comparison of the simulated results of hydrogen sparging with and without foam in a hypothetical heterogeneous aquifer. The aquifer is 20 ft in depth with a 5 ft vadose zone above it. It has two layers of high permeability sand (200 darcy) in the lower part of it (1.5 ft and 4.5 ft from the bottom correspondingly). The rest of the aquifer is 40 darcy sand. Hydrogen is injected from the bottom of the aquifer using a 8 psi over hydrostatic pressure. Because of the hazard of hydrogen mixed with air, our comparisons will be based on simulated results up to the breakthrough time of hydrogen. From the comparison we can see that the effect of foam is obvious, in the foam case hydrogen can propagate about 20 ft long in the diagonal cross section before breakthrough but only about 7.5 ft in the without foam case. In another case study of a hypothetical homogeneous aquifer[27], foam can also greatly improve the hydrogen sweep along the bottom of the aquifer, though the difference between with and without foam is not as great as in the heterogeneous aquifer.

Conclusions

From the studies of 3-D foam experiments and simulations, we can obtain the following conclusions:

1. Foam can greatly reduce the gas mobility and increase the gas sweep efficiency and average gas saturation in the 3-D tank.
2. Injection pressure is very important when applying a foam process. It should be high enough to generate strong foam and get good gas sweep efficiency.

3. For a gas sparging process with foam, the intermittent injection method can result in the best gas sweep efficiency and average gas saturation.
4. Foam has shear thinning effect near the injection well because of the high flow rate and this will aid injectivity.
5. The heterogeneity in the lower part of the tank can benefit the horizontal transport of foam and increase the gas sweep efficiency.
6. The proposed foam model can successfully history match and simulate the 1-D and 3-D foam results. Parameters can be obtained from 1-D experiments and applied to 3-D simulations.
7. The experimental and the simulation results show that foam is weaker in 3-D than in 1-D. In simulation, the difference between 1-D and 3-D can be represented by using the geometry factor F_g , which is about 5 times smaller in 3-D than in 1-D.
8. To extend to field simulation, an equivalent pressure gradient should be determined from the injection pressure and the shear thinning effect between the injection well and the grid block should be incorporated. The hypothetical field simulations show that gas sweep can be greatly improved by foam in the field scale.

Acknowledgment

We acknowledge the Strategic Environmental Research and Development Program (SERDP) for the financial support of this research. Also, we acknowledge Dr. Mojdeh Delshad and Dr. Gary Pope from UT Austin on providing us the UTCHEM source codes and giving suggestions on the codes modification.

Nomenclature

$C_{nf}, C_{\mu f}$ = constant coefficient
e_l = exponent of the relative permeability curve of phase l
F_g = geometry factor
k = permeability, L^2, darcy
k_{rl} = relative permeability of phase l
k_{rl}^0 = relative permeability end point of phase l
k_{rg}^f = relative permeability of gas when foam is present
LPM = Liter Per Minute
m = exponent of the gas saturation effect
n = exponent of the shear thinning effect
n_f = lamellae density
P_c = capillary pressure, m/Lt^2, psi
P_c^* = limiting capillary pressure, m/Lt^2, psi
∇p = pressure gradient, m/Lt^2, psi
PV = pore volume
S_l = saturation of phase l
S_{rl} = residual saturation of phase l
S_{rg}^f = gas residual saturation when foam is present
S_{gm} = reference gas saturation
S_g^* = gas saturation at limiting capillary pressure
u_g = gas superficial (Darcy) velocity, L/t, ft/day
u_{ref} = reference gas superficial velocity, L/t, ft/day
v_g = interstitial gas phase velocity, L/t, ft/day
v_{ref} = reference interstitial gas phase velocity, L/t, ft/day
ϕ = porosity
μ_g = viscosity of gas, m/Lt, cp
μ_g^f = viscosity of gas when foam is present, m/Lt, cp

References

1. Hirasaki, G.J., Miller, C.A., Szafranski, R., Lawson, J.B., and Akiya, N.: "Surfactant/Foam Process for Aquifer Remediation," paper SPE 37257 presented at the SPE International Symposium on Oilfield Chemistry, Houston, Texas, 18-21 February 1997.
2. Hirasaki, G.J., Miller, C.A., Szafranski, R., Tanzil, D., Lawson, J.B., Meinardus, H., Jin, M., Londergan, J.T., Jackson, R.E., Pope, G.A., and Wade, W.H.: "Field Demonstration of the Surfactant/Foam Process for Aquifer Remediation," paper SPE 39292 presented at the 1997 Annual Technical Conference and Exhibition, San Antonio, Texas, 5-8 October.
3. Szafranski, R., Lawson, J.B., Hirasaki, G.J., Miller, C.A., Akiya, N., King, S., Jackson, R.E., Meinardus, H., and Londergan, J.: "Surfactant/foam process for improved efficiency of aquifer remediation," *Prog. Colloid Polym. Sci.* (1998), 111, 162-167.
4. Hirasaki, G.J., Jackson, R.E., Jin, M., Lawson, J.B., Londergan, J., Meinardus, H., Miller, C.A., Pope, G.A., Szafranski, R., and Tanzil, D.: "Field demonstration of the surfactant/foam process for remediation of a heterogeneous aquifer contaminated with DNAPL," in *NAPL Removal: Surfactants, Foams, and Microemulsion*, Fiorenza, S., Miller, C.A., Oubre, C.L., and Ward, C.H., eds., CRC Press, Boca Raton (2000).
5. Hirasaki, G.J.: "The Steam-Foam Process," *JPT* (May 1989), 449-456.
6. Liu, D., Castanier, L.M., and Brigham, W.E.: "Displacement by Foam in Porous Media," paper SPE 24664 presented at the 67th Annual Technical Conference and Exhibition, Washington, DC, October 4-7, 1992.
7. Patzek, T.W.: "Field Application of Steam Foam for Mobility Improvement and Profile Control," *SPE RE* (1996), 11, 79-85.
8. Blaker, T., Celius, H.K., Lie, T., Martinsen, H.A., Rasmussen, L., and Vassenden, F.: "Foam for Gas Mobility Control in the Snorre Field: The FAWAG Project," paper SPE 56478 presented at the 1999 SPE Annual Conference and Exhibition, Houston, Texas, 3-6 October.
9. Tanzil, D.: "Foam Generation and Propagation in Heterogeneous Porous Media," Ph.D. dissertation, Rice U., 2001
10. Hirasaki, G.J.: "Supplement to SPE 19505, The Steam-Foam Process—A Review of Steam-Foam Process Mechanisms," paper SPE19518, available from SPE, Richardson, Texas (1989).
11. Rossen, W. R., and Gauglitz, P. A.: "Percolation Theory of Creation and Mobilization of Foam in Porous Media", *AICHE J*. 36 (1990), 1176-1188.
12. Tanzil, D., Hirasaki, G. J. and Miller, C.A.: " Conditions for Foam Generation in Homogeneous Porous Media", paper SPE 75176 presented at the SPE/DOE Thirteenth Symposium on Improved Oil Recovery held in Tulsa, Oklahoma, 13-17 April 2002.
13. Gauglitz, P.A., Friedmann, F., Kam, S. I., and Rossen, W.R.: "Foam Generation in Porous Media", paper SPE 75177 presented at the SPE/DOE Thirteenth Symposium on Improved Oil Recovery held in Tulsa, Oklahoma, 13-17 April 2002.
14. Li,Q. and Rossen, W.R.: "Injection Strategies for Foam Generation in Homogeneous and Layered Porous Media",

paper SPE 96116 presented at the 2005 SPE Annual Conference and Exhibition, Dallas, Texas.
15. Khatib, Z.I., Hirasaki, G.J., and Falls, A.H.: "Effects of Capillary Pressure on Coalescence and Phase Mobilities in Foams Flowing Through Porous Media," *SPERE* (August 1988) 919.
16. Bernard, G. G., Holm, L. W., and Jacobs, W. L.: "Effect of Foam on Trapped Gas Saturation and on Permeability of Porous Media to Water", *SPE J*, Dec.1965, 195-300.
17. Holm, L. W.: "The mechanisms of Gas and Liquid Flow Through Porous Media in the Presence of Foam", *SPEJ*, Dec. 1968, 359-369.
18. Hirasaki, G. J., and Lawson, J. B.: "Mechanisms of Foam Flow in Porous Media: Apparent Viscosity in Smooth Capillaries", *SPEJ*, Apr. 1985, Vol. 25, No.2, 176-190.
19. Falls, A.H., G.J. Hirasaki, T.W. Patzek, D.A. Gauglitz, D.D. Miller, and T. Ratulowski. "Development of a mechanistic foam simulator: the population balance and generation by snap-off," *SPE Reservoir Engineering*, August 1988, 884-892.
20. Kovscek, A. R., Patze, T.W., Radke, C. J.: "Mechanistic Prediction of Foam Displacement in Multidimensions: A Population-Balance Approach," paper SPE 27789 presented at the 1994 SPE/DOE Symposium on Improved Oil Recovery, Tulsa, OK.
21. Hatzlavramidls, D. T. *et al*: "A Mechanistic Foam Model for Simulation of Steam Foam Field Applications," paper SPE 30728 presented at the Annual Technical Conference and Exhibition of the SPE, Dallas (1995).
22. Bertin, H.J., M.Y. Quintard, and L.M. Castanier. "Development of a bubble-population correlation for foam-flow modeling in porous media," *SPE J.*, December 1998b, 356-362.
23. Friedmann, F., Chen, W.H., and Gauglitz, P.: "Experimental and Simulation Study of High-Temperature Foam Displacement in Porous Media," *SPERE* (February 1991) 37.
24. Falls, A. H., Musters, J. J., and Ramdowski, J.: "The Apparent Viscosity of Foams in Homogeneous Bead Packs," *SPERE* (May 1989) 155-64.
25. Tanzil, D., Hirasaki, G. J. and Miller, C.A.: " Mobility of Foam in Heterogeneous Media: Flow Parallel and Perpendicular to Stratification", *SPEJ*. 7 (2002), 203-212
26. Shi, J.-X. and W.R. Rossen. "Improved surfactant-alternating-gas foam process to control gravity override," paper SPE 39653, presented at the 1998 SPE/DOE Improved Oil Recovery Symposium, Tulsa, OK, 19-22 April 1998.
27. Li, B.: "Surfactant/Foam Enhanced Aquifer Contacting and Modeling for Aquifer Remediation," Ph.D. dissertation, Rice U., 2006
28. Bondor, P.L., Hirasaki, G.J. and Tham, M.J. "Mathematical Simulation of Polymer Flooding in Complex Reservoirs," *SPEJ*. 10 (1972)

Table 1 Parameters determined from 1-D column experiments

1-D column	Injection pressure	S_{rg}^{f}	u_{ref}	n	S_{gm}	m	$C_{\mu f}$
40 darcy	0.4 psi	0.4	2 ft/day	0.2	0.80	5	4,500
	0.2 psi	0.4	2 ft/day	0.2	0.80	5	2,700
200 darcy	0.4 psi	0.7	6 ft/day	0.4	0.85	12	1,200
	0.2 psi	0.7	6 ft/day	0.4	0.85	12	650

Table 2 Comparison of simulated and experimental gas saturation in 1-D column

0.05%CS-330 0.05%C13-4PO fg=100%		40 darcy sand column		200 darcy sand column	
		0.4 psi	0.2 psi	0.4 psi	0.2 psi
Sg	Experimental	82%	79%	85%	85%
	Simulated	84%	72%	86%	84%

Table 3 Comparison of parameters for 1-D and 3-D simulation

			S^f_{rg}	u_{ref}	n	S_{gm}	m	$C_{\mu f}$	F_g
Homogeneous Sand Pack (40 darcy)									
0.4 psi constant injection pressure (**1-D column, 1 ft**)			0.4	2	0.2	0.80	5	4,500	1.00
0.8 psi constant injection pressure (**3-D tank, 2x2x2 ft**)			0.4	2	0.2	0.80	5	4,500	0.21
0.2 psi constant injection pressure (**1-D column, 1 ft**)			0.4	2	0.2	0.80	5	2,700	1.00
0.39LPM constant rate (~0.4 psi injection pressure) (**3-D tank, 2x2x2 ft**)			0.4	2	0.2	0.80	5	2,700	0.21
Heterogeneous Sand Pack (40&200 darcy)									
Case 1: 0.8psi constant injection pressure	High perm (200 darcy)	0.4 psi (**1-D** column)	0.7	6	0.4	0.85	12	1,200	1.00
		3-D sand tank	0.7	6	0.4	0.85	12	3,100	0.21
	Low perm (40 darcy)		0.4	2	0.2	0.80	5	4,500	0.21
Case 2: 0.4psi constant injection pressure	High perm (200 darcy)	0.2 psi (**1-D** column)	0.7	6	0.4	0.85	12	650	1.00
		3-D sand tank	0.7	6	0.4	0.85	12	2,140	0.21
	Low perm (40 darcy)		0.4	2	0.2	0.80	5	4,000	0.21

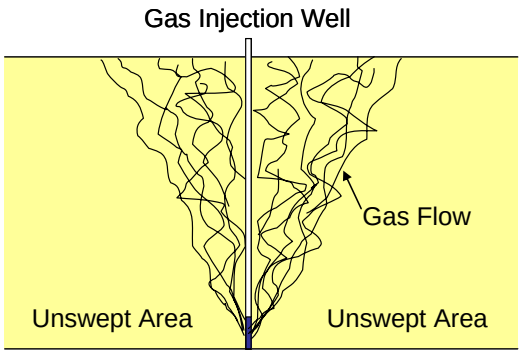

Fig. 1 Problem of a regular gas injection process

Fig.2 An overlook of the 3-D tank (before sand packing)

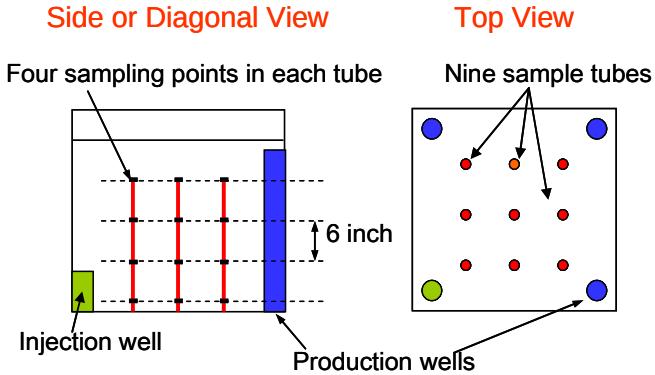

Fig. 3 Sketches of the side and top views of the tank

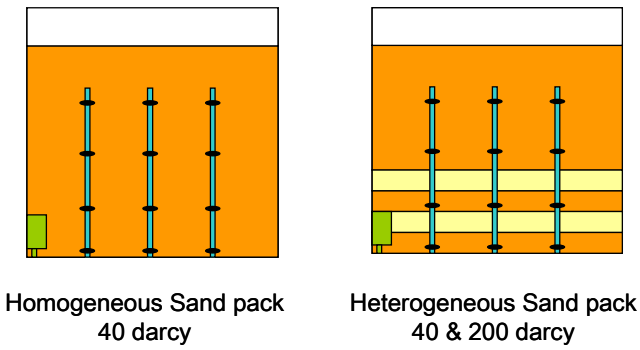

Fig. 4 Two sand pack formations

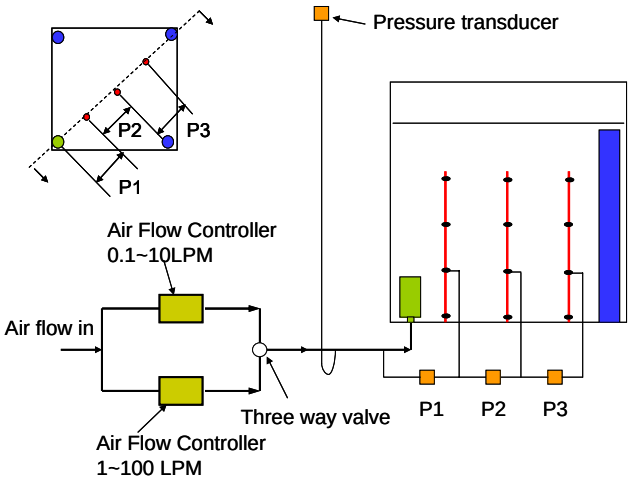

Fig. 5 Experimental outlines of the 3-D tank

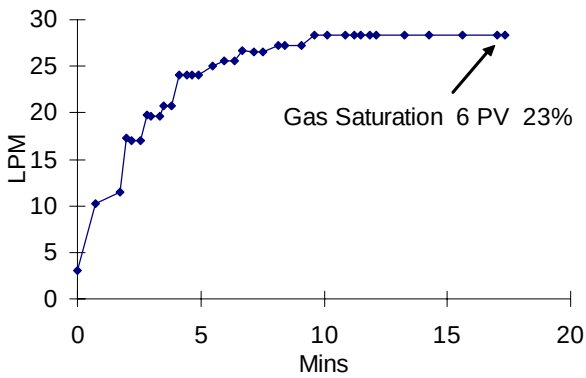

Fig. 6 Air/Water, Homogeneous sand tank, Curve of injection rate; Constant injection pressure ~0.8 psi, 6 PV gas injected

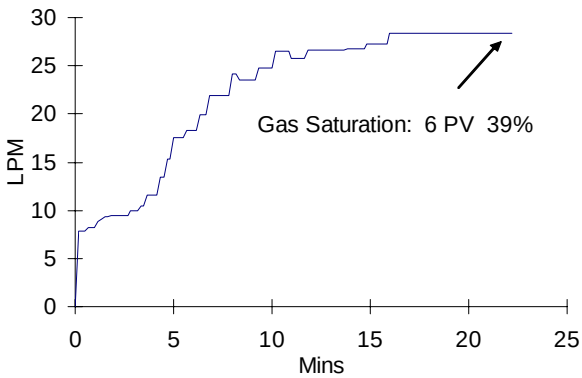

Fig.7 Air/water, Heterogeneous sand tank, Curve of Injection rate; Continuous injection pressure ~0.8 psi, 6 PV gas injected

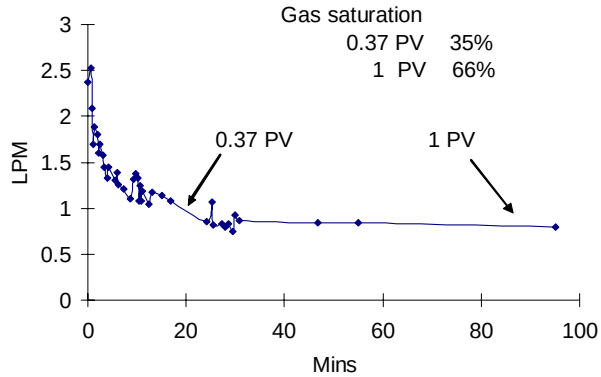

Fig. 8 Foam; Homogeneous sand tank; Curve of injection rate; Constant injection pressure ~0.8 psi; 1 PV gas injected

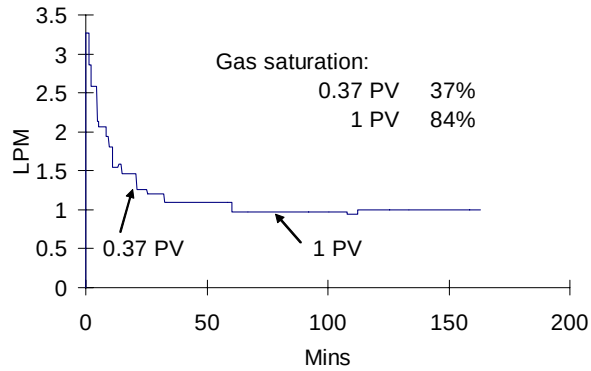

Fig. 9 Foam; Heterogeneous sand tank; Curve of injection rate; Constant injection pressure ~0.8 psi, 1 PV gas injected

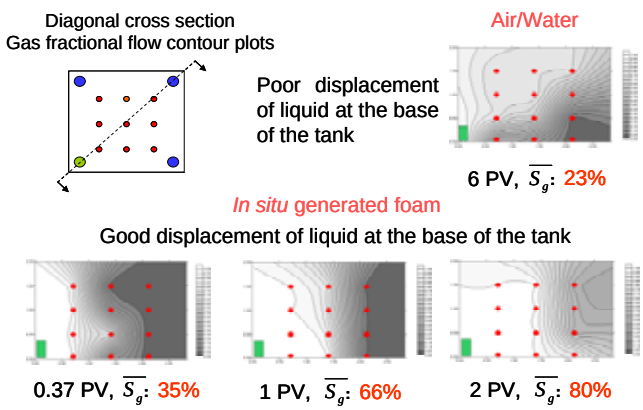

Fig. 10 Comparison of air/water and foam results along the diagonal cross section of the tank, Homogeneous Tank Constant injection pressure ~0.8 psi

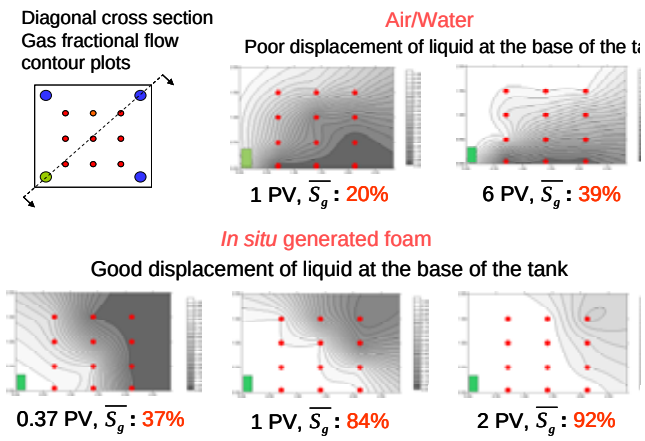

Fig. 11 Comparison of air/water and foam results along the diagonal cross section of the tank, Heterogeneous Tank Constant injection pressure ~0.8 psi

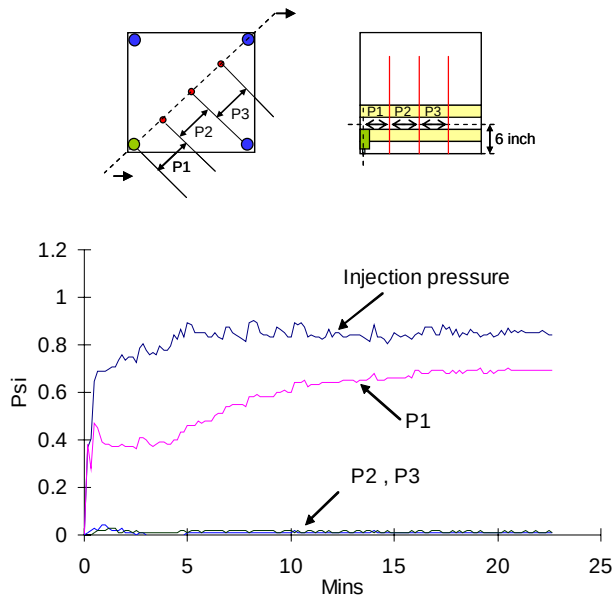

Fig. 12.A Air/Water; Heterogeneous pack, Constant injection pressure ~0.8 psi, Pressure profiles along the diagonal cross section of the tank

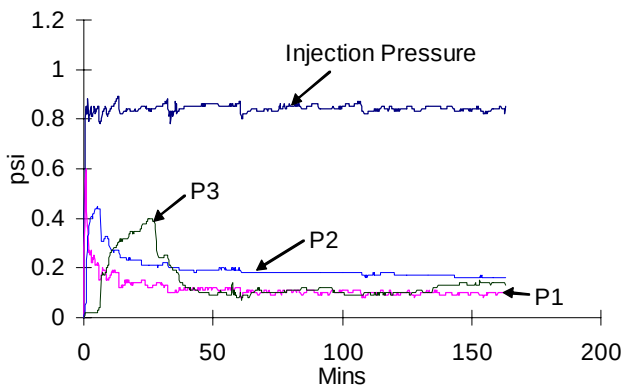

Fig. 12.B Foam; Heterogeneous pack, Constant injection pressure ~0.8 psi, Pressure profiles along the diagonal cross section of the tank

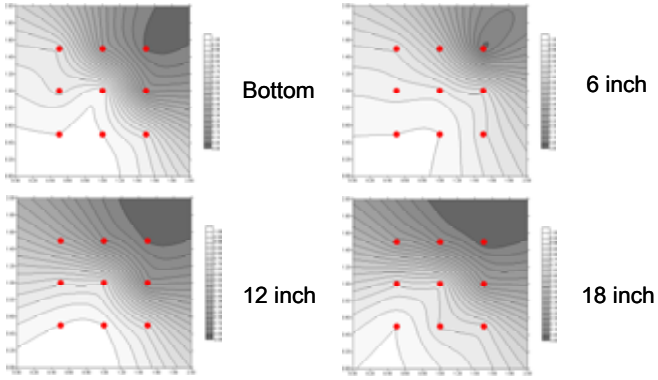

Fig.13 Foam, Homogeneous sand tank, gas fraction flow contour plot, Continuous gas injection, ~0.8 psi, ~1 PV gas injected

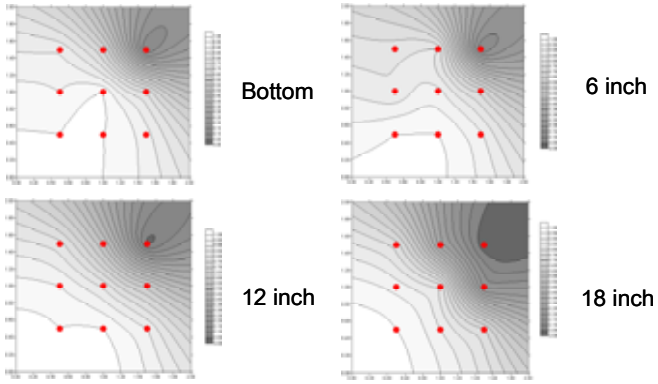

Fig. 14 Foam, Homogeneous sand tank, gas fraction flow contour plot, Intermittent gas injection, ~0.8 psi, ~1 PV gas injected

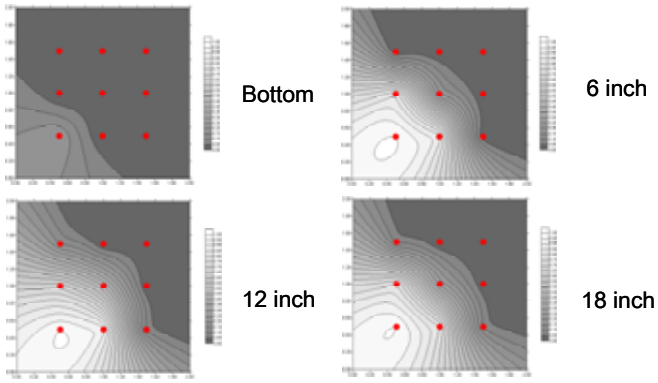

Fig. 15 Foam, Homogeneous sand tank, gas fraction flow contour plot, lower injection pressure, ~0.4 psi, ~1 PV gas injected

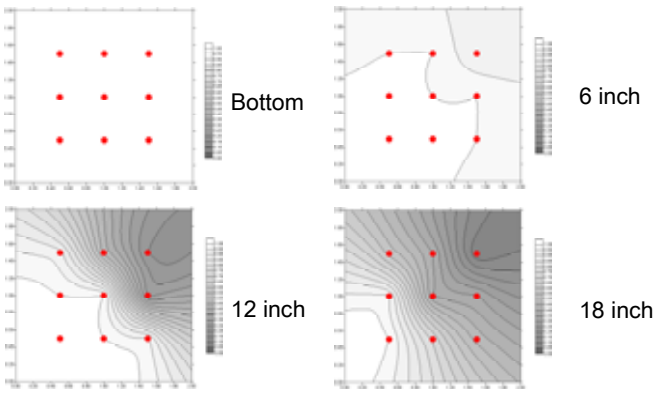

Fig.16 Foam, Heterogeneous sand tank, gas fraction flow contour plot, Continuous gas injection, ~0.8 psi, ~1 PV gas injected

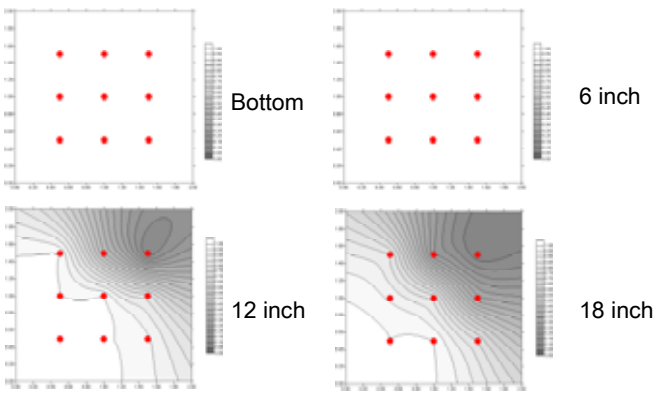

Fig. 17 Foam, Heterogeneous sand tank, gas fraction flow contour plot, Intermittent gas injection, ~0.8 psi, ~1 PV gas injected

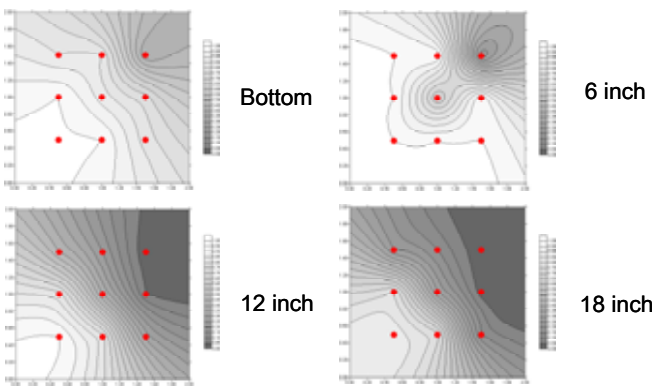

Fig. 18 Foam, Heterogeneous sand tank, gas fraction flow contour plot, lower injection pressure, ~0.4 psi, ~1 PV gas injected

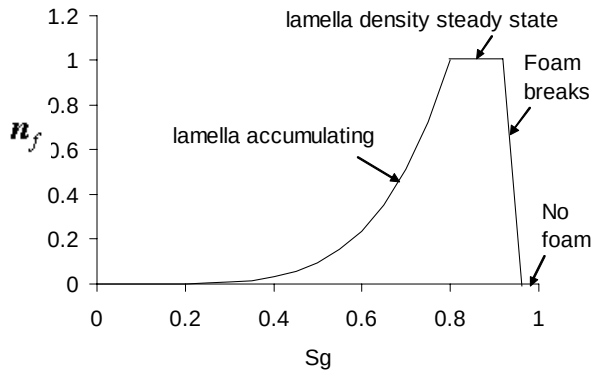

Fig. 19 Relationship between Sg and n_f

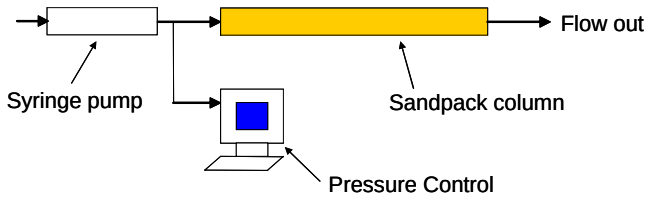

Fig. 20 1-D column experiment set up

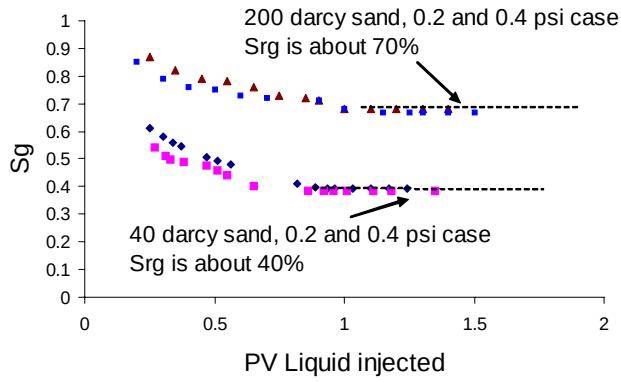

Fig. 21 Gas residual saturation measurement using 1-D column

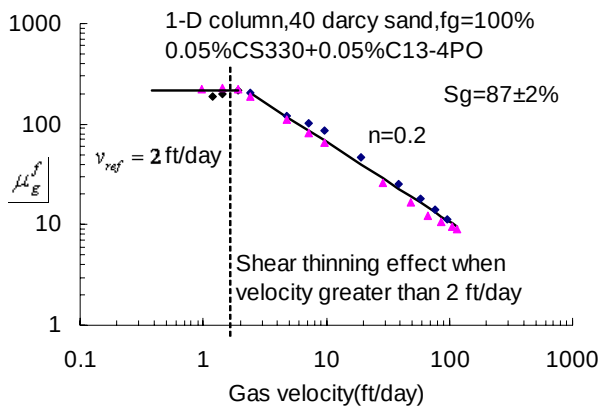

Fig. 22 Foam shear thinning effect at high velocity, 40 darcy sand

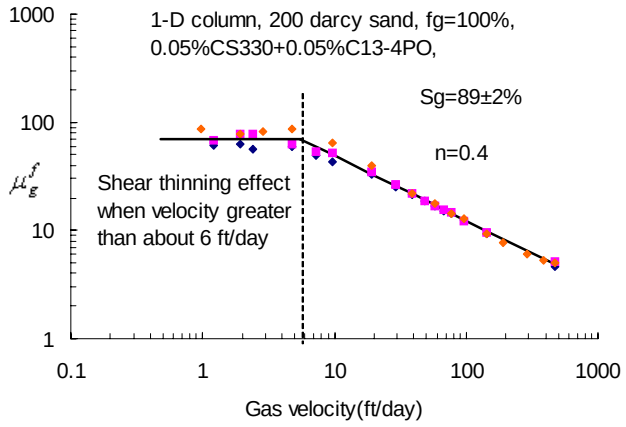

Fig. 23 Foam shear thinning effect at high velocity, 200 darcy sand

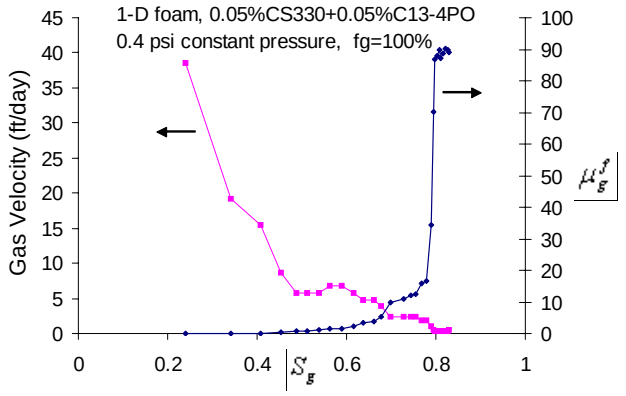

Fig.24 Gas saturation vs. foam effective viscosity and gas superficial velocity, 40 darcy sand, 0.4 psi constant injection

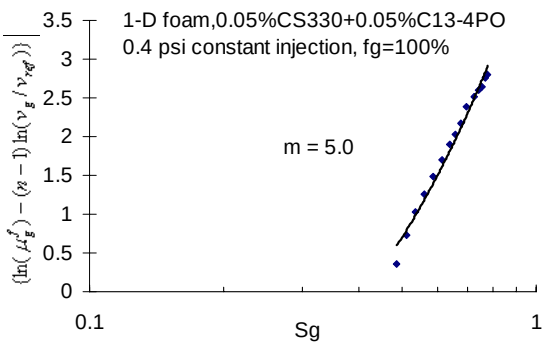

Fig. 25 Relationship between foam effective viscosity and gas saturation 40 darcy sand, 0.4 psi constant injection

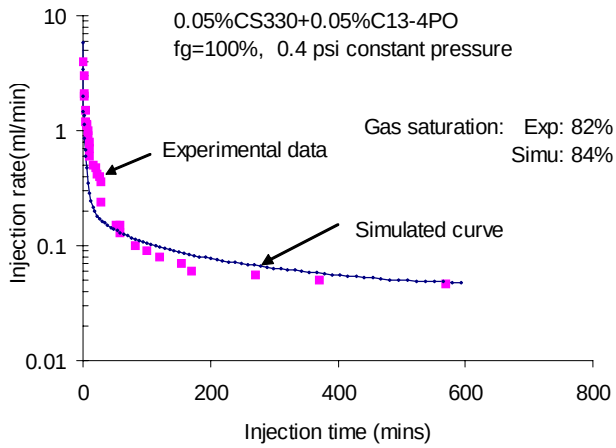

Fig. 26 1-D column simulation results vs. experimental data 40 darcy sand, 0.4 psi constant injection pressure

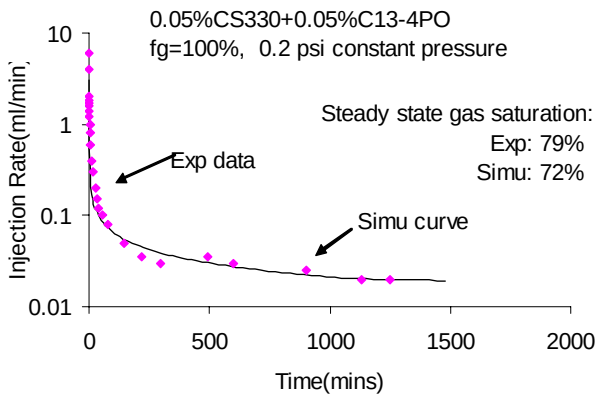

Fig. 27 1-D column simulation results vs. experimental data 40 darcy sand, 0.2 psi constant injection pressure

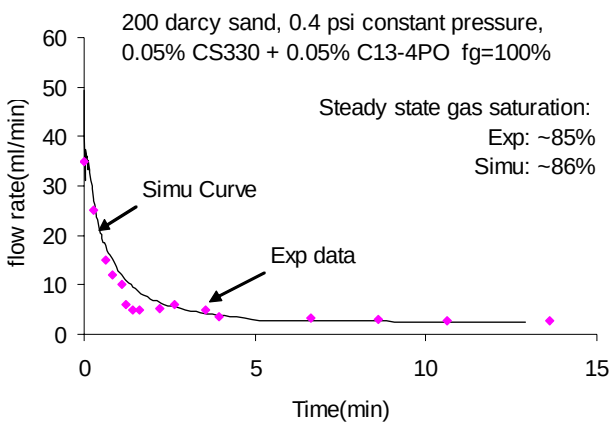

Fig. 28 1-D column simulation results vs. experimental data 200 darcy sand, 0.4 psi constant injection pressure

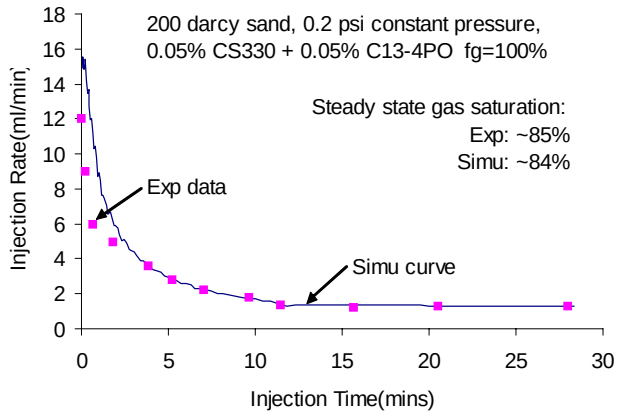

Fig. 29 1-D column simulation results vs. experimental data 200 darcy sand, 0.2 psi constant injection pressure

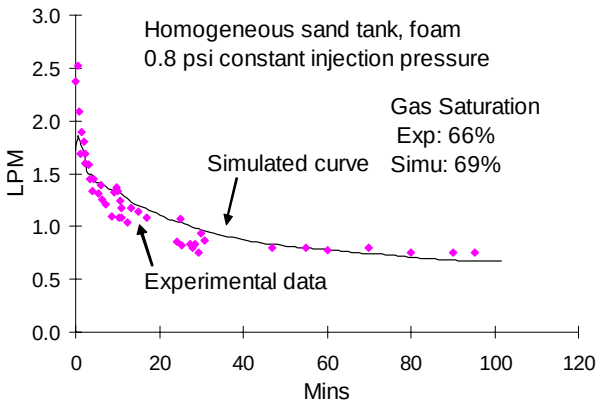

Fig. 30 Homogeneous 3-D sand tank, 40 darcy, 0.8 psi constant injection pressure

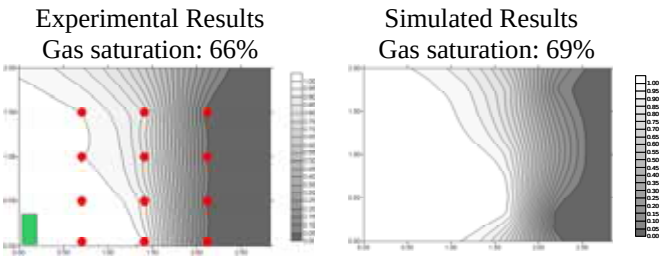

Fig. 31 Homogeneous 3-D sand tank, Cross section gas fractional flow contour plots, 40 darcy, 0.8 psi constant injection pressure

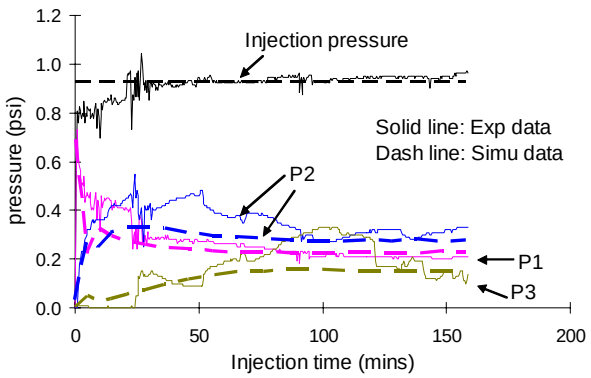

Fig. 32 Homogeneous 3-D sand tank, foam, pressure profile, 0.8 psi constant injection pressure

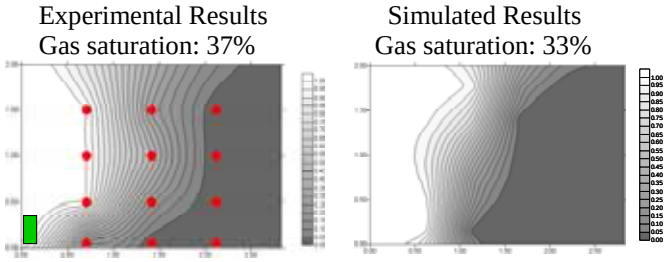

Fig. 33 Gas fractional flow contour plots, diagonal cross section, 0.4psi (0.39 LPM constant injection rate), 1 PV gas injected

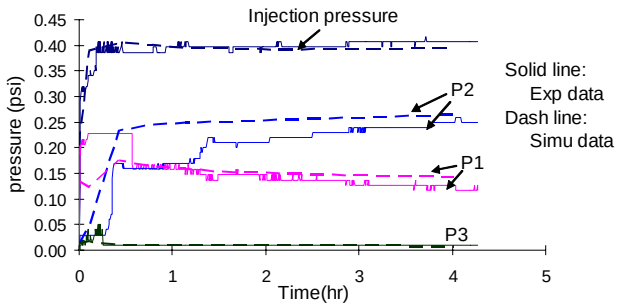

Fig. 34 Homogeneous Sand Tank, 0.4 psi (0.39LPM constant injection rate), pressure profile

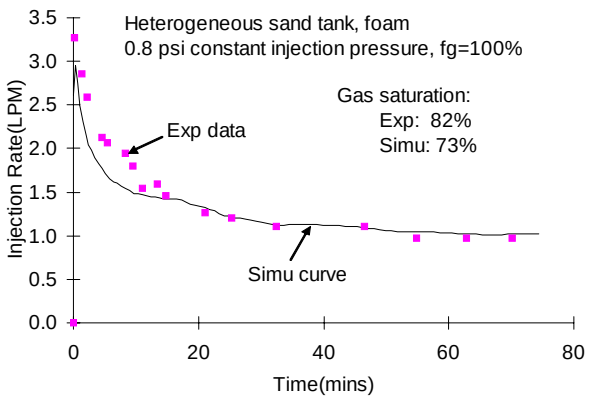

Fig. 35 Heterogeneous 3-D sand tank, 0.8 psi constant injection pressure, 1 PV gas injected

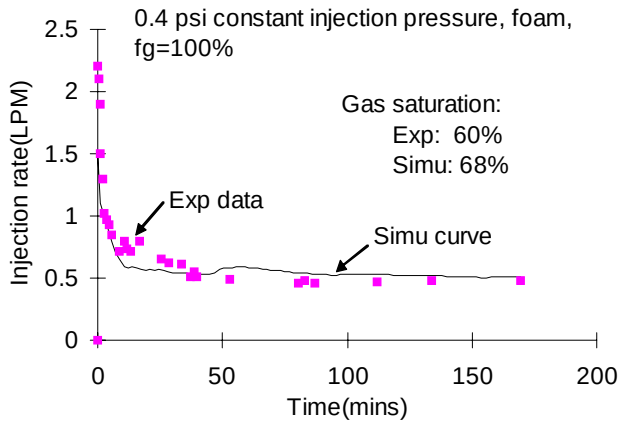

Fig. 38 Heterogeneous 3-D sand tank, 0.4 psi constant injection pressure

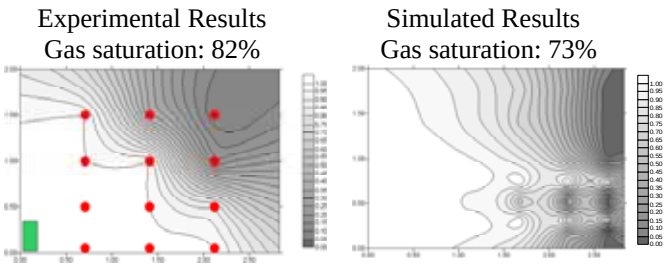

Fig. 36 Heterogeneous 3-D sand tank, Cross section gas fractional flow contour plots, 0.8 psi constant injection pressure

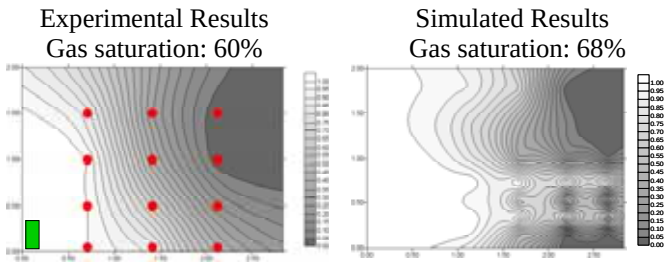

Fig. 39 Heterogeneous 3-D sand tank, Cross section gas fractional flow contour plots, 0.4 psi constant injection pressure

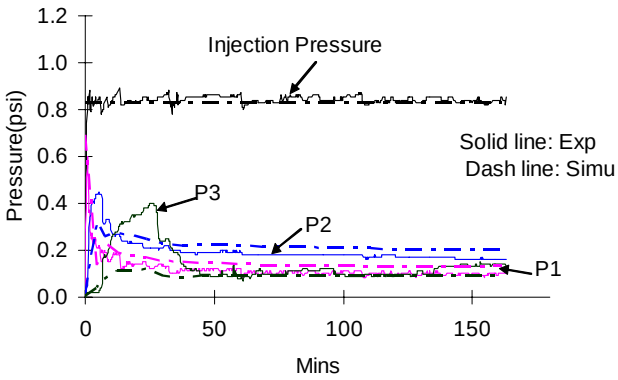

Fig. 37 Heterogeneous 3-D sand tank, 0.8 psi constant injection pressure, pressure profile

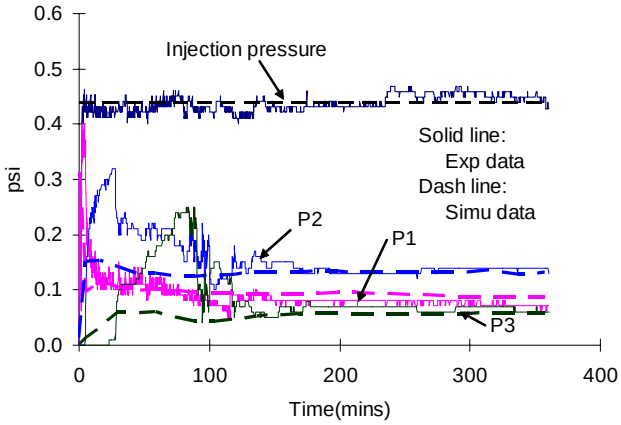

Fig. 40 Heterogeneous 3-D sand tank, 0.4 psi constant injection pressure, pressure profile

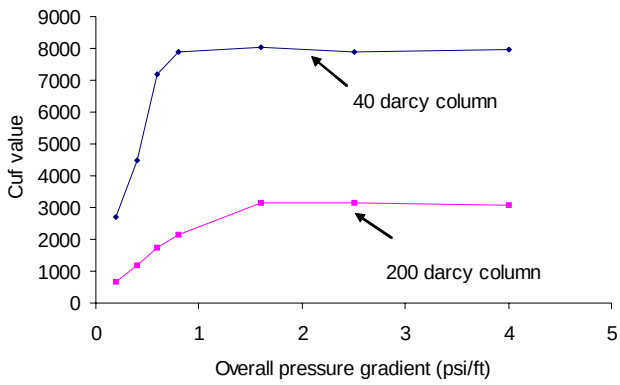

Fig. 41 The change of C_{uf} value with the change of pressure gradient

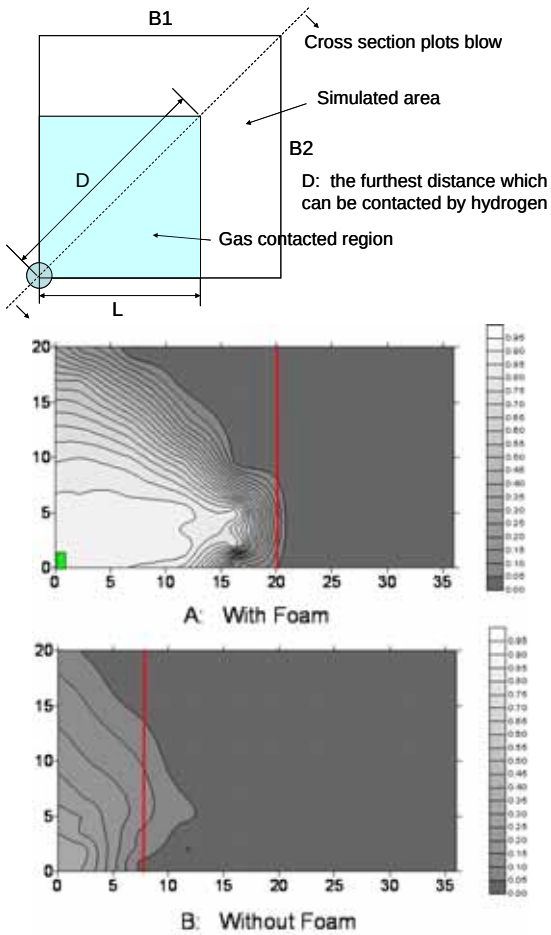

Fig. 42 Gas saturation contour plots for with and without foam cases, hypothetical heterogeneous aquifer